Characterization of Covalent Linkages in Organically Functionalized MCM-41 Mesoporous Materials by Solid-State NMR and Theoretical Calculations

ARTICLE *in* THE JOURNAL OF PHYSICAL CHEMISTRY B · MAY 2007

Impact Factor: 3.3 · DOI: 10.1021/jp067417x · Source: PubMed

7 AUTHORS, INCLUDING:

Niladri Maity
King Abdullah University of Science and Tech…
11 PUBLICATIONS **91** CITATIONS
SEE PROFILE

Sumit Bhaduri
Indian Institute of Technology Bombay
137 PUBLICATIONS **1,898** CITATIONS
SEE PROFILE

Subramanian Ganapathy
CSIR - National Chemical Laboratory, Pune
18 PUBLICATIONS **273** CITATIONS
SEE PROFILE

Characterization of Covalent Linkages in Organically Functionalized MCM-41 Mesoporous Materials by Solid-State NMR and Theoretical Calculations

Jerzy W. Wiench,[†] Yamini S. Avadhut,[‡] Niladri Maity,[§] Sumit Bhaduri,*[,||] Goutam Kumar Lahiri,[§] Marek Pruski,*[,†] and Subramanian Ganapathy*[,‡]

Ames Laboratory and Department of Chemistry, Iowa State University, Ames, Iowa 50011-3020, Central NMR Facility, National Chemical Laboratory, Pune 411008, India, Department of Chemistry, Indian Institute of Technology Bombay, Powai, Mumbai 400076, India, and Reliance Industries Limited, Swastik Mills Compound, V.N. Purav Marg, Chembur, Mumbai 400071, India

Received: November 9, 2006; In Final Form: January 6, 2007

The covalent linkages formed during functionalization of MCM-41 mesoporous molecular sieves with five chloroalkylsilanes ($(EtO)_3Si(CH_2Cl)$, $(MeO)_3Si(CH_2CH_2CH_2Cl)$, $Cl_3Si(CH_2CH_2CH_3)$, $Cl_2Si(CH_3)(CH_2Cl)$ and $Cl_2Si(CH_3)_2$) have been investigated using high-resolution solid-state NMR spectroscopy and DFT calculations. Structural information was obtained from $^1H-^{13}C$ and $^1H-^{29}Si$ heteronuclear (HETCOR) NMR spectra, in which high resolution in the ^1H dimension was obtained by using fast MAS. The $^1H-^{13}C$ HETCOR results provided the assignments of ^1H and ^{13}C resonances associated with the surface functional groups. Sensitivity-enhanced $^1H-^{29}Si$ HETCOR spectra, acquired using Carr−Purcell−Meiboom−Gill refocusing during data acquisition, revealed the identity of ^{29}Si sites (Q^n, T^n, and D^n) and the location of functional groups relative to these sites. Optimal geometries of local environments representing the Q^n, T^n and D^n resonances were calculated using molecular mechanics and *ab initio* methods. Subsequently, DFT calculations of ^{29}Si, ^{13}C, and ^1H chemical shifts were performed using Gaussian 03 at the B3LYP/6-311++G(2d,2p) level. The theoretical calculations are in excellent accord with the experimental chemical shifts. This work illustrates that state-of-the-art spectroscopic and theoretical tools can be used jointly to refine the complex structures of inorganic−organic hybrid materials.

Introduction

There is considerable current interest in the functionalization of supramolecular-templated mesoporous inorganic silica materials using organic groups tailored for various applications in separation,[1−3] drug delivery,[4] sensor design,[5,6] and catalysis.[7−14] The textural characteristics of the inorganic frameworks in such materials can be controlled using a variety of synthetic methods, while tethering of the organic groups offers opportunities for further modification. In catalytic applications, surface functionalization can be used to stabilize the active sites, control the selectivity, and promote adsorption/desorption of the reacting species. The most commonly used mesoporous silica is MCM-41, synthesized from a silica source (e.g., tetraethylorthosilicate, TEOS), in presence of a surfactant (e.g., cetyltrimethylammonium bromide, CTAB), and a base (e.g., sodium hydroxide), in water solution.[15] The surfactant molecules form supramolecular assemblies, which template the inorganic component (silica). The resulting MCM-41 framework consists of non-intersecting, hexagonally packed cylindrical mesopores, whose width can be modified by changing the length of the template molecule. The walls of the channels are composed of amorphous SiO_2, which makes MCM-41 mechanically stable in spite of its exceptional porosity (up to 80%). The core of MCM-41 walls consists of silicon sites referred to as Q^4, which are connected to four Si neighbors via siloxane linkages ($(\equiv SiO)_4\mathbf{Si}$). In nonfunctionalized materials, silica surfaces are terminated by the silanol groups (SiOH), forming Q^3 sites, $(\equiv SiO)_3\mathbf{Si}(OH)$, and Q^2 sites, $(\equiv SiO)_2\mathbf{Si}(OH)_2$. These sites can be described by the general formula $(\equiv SiO)_n\mathbf{Si}R_mX_{4-n-m}$, where $m = 0$ and X = OH. Functionalization of the silica surface is usually carried out via postsynthesis grafting (after the removal of the surfactant)[16,17] or through co-condensation.[18−24] In addition to Q^n sites, the functionalized materials may contain silicon atoms in positions denoted as T^n ($m = 1$; $n = 0, 1, 2, 3$) and D^n ($m = 2$; $n = 0, 1, 2$), where X = OH, OCH_3, Cl, etc.[25]

Identification of these groups and their structures is an important challenge. The templated mesoporous silicas are usually uniform but never crystalline and thus cannot be examined in depth with X-ray diffraction. Solid-state NMR spectroscopy, on the other hand, is ideally suited for studies of such high-surface materials.[24,26−35] In the nonfunctionalized samples, one-dimensional (1D) ^{29}Si magic-angle spinning NMR spectra obtained with direct polarization (MAS) or $^1H-^{29}Si$ cross polarization (CPMAS) are used to identify and quantify the Q^n silicon sites. The degree of functionalization can be quantitatively assessed using ^{29}Si MAS spectra, while $^1H-^{13}C$ CPMAS measurements can identify the functional groups. More accurate information about the structure, topology, and dynamics of surface functionalities is provided by two-dimensional (2D) methods that correlate the chemical shifts of neighboring spins. We have recently demonstrated that 2D heteronuclear correlation (HETCOR) $^1H-^{29}Si$ and $^1H-^{13}C$ spectra can be conveniently observed on functionalized silica surfaces by using fast MAS.[33−35] Since the static ^1H NMR line widths in such samples are

* To whom correspondence should be addressed. E-mail: mpruski@iastate.edu (M.P.); s.ganapathy@ncl.res.in (S.G.).
[†] Iowa State University.
[‡] National Chemical Laboratory.
[§] Indian Institute of Technology Bombay.
[||] Reliance Industries Limited.

10.1021/jp067417x CCC: $37.00
Published on Web 03/28/2007

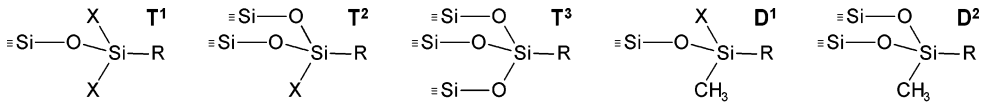

Sample	Reagent		Si site	R	X
1	$(CH_3CH_2O)_3Si(CH_2Cl)$	CMTES	T^n	CH_2Cl	OH or OCH_2CH_3
2	$(CH_3O)_3Si(CH_2CH_2CH_2Cl)$	CPTMS	T^n	$CH_2CH_2CH_2Cl$	OH or OCH_3
3	$Cl_3Si(CH_2CH_2CH_3)$	PTCS	T^n	$CH_2CH_2CH_3$	OH or Cl
4	$Cl_2Si(CH_3)(CH_2Cl)$	CMDCMS	D^n	CH_2Cl	OH or Cl
5	$Cl_2Si(CH_3)_2$	DMDCS	D^n	CH_3	OH or Cl

Figure 1. Environments anticipated in the present study for the silicon sites functionalized with CMTES, CPTMS, PTCS, CMDCMS, and DMDCS. Following ref 25, the functionalized environments $(\equiv SiO)_n\mathbf{Si}R_mX_{4-n-m}$ are denoted as T^n ($m = 1$; $n = 0, 1, 2, 3$, X = OH, OCH_3, OCH_2CH_3, or Cl) and D^n ($m = 2$; $n = 0, 1, 2$, X = OH or Cl), where n is the number of covalent linkages of the organic moiety to the host.

typically reduced to below 20 kHz due to molecular motion, MAS at 40 kHz can provide excellent $^1H-^1H$ decoupling, whereas at these spinning frequencies multipulse $^1H-^1H$ decoupling becomes inherently less effective. Additional advantages of using fast MAS in HETCOR NMR include easy setup, lack of scaling factors, and ease of acquisition of sideband-free spectra. The loss of signal to small rotor volume (less than 5 mg of sample) is compensated by the higher sensitivity per spin.[34] Indeed, we have obtained 2D $^1H-^{13}C$ HETCOR NMR spectra of several functional groups on silica without using isotope enrichment.[34,35] In addition, the $^1H-^{29}Si$ HETCOR experiments under fast MAS can be made routine by applying the CPMG train of π pulses to the ^{29}Si spins, which increases the sensitivity by as much as 1 order of magnitude.[34]

While the aforementioned experimental methods provide increasingly accurate structural data, theoretical modeling offers additional means for more incisive characterization. The geometrical arrangements of atoms at the functionalized sites have a considerable effect on the local electronic environment and the chemical shielding anisotropy (CSA) tensors ($\boldsymbol{\sigma}$) of neighboring ^{29}Si, ^{13}C, and ^1H nuclei. The cluster models, which represent the different possible functionalized environments (T^n and D^n sites), can be optimized using molecular mechanics and ab initio methods. The CSA tensors are then calculated on the basis of density functional theory (DFT). The theoretical isotropic chemical shifts can be correlated with the results of HETCOR experiments to validate the proposed structures.

We describe herein a detailed investigation of the covalent linkages formed in organically functionalized MCM-41 silica materials using comprehensive characterization by solid-state NMR spectroscopy in conjunction with DFT calculations of the ^{29}Si, ^{13}C, and ^1H chemical shielding. We demonstrate that the combination of state-of-the-art spectroscopic and theoretical tools can indeed be used to refine the complex structures of inorganic−organic hybrid materials. The organic compounds used in this study involve five different silanes, which were chosen because of their utility as coupling agents for immobilization of catalytically active complexes.[36,37]

Materials and Methods

Preparation of Functionalized MCM-41 Materials. MCM-41 was synthesized according to the literature reported procedure.[15,38] The alkylsilanes used for functionalization were purchased from Aldrich. They included chloromethyltriethoxysilane ($(EtO)_3Si(CH_2Cl)$, referred to as CMTES), chloropropyltrimethoxysilane ($(MeO)_3Si(CH_2CH_2CH_2Cl)$, CPTMS), *n*-propyltrichlorosilane ($Cl_3Si(CH_2CH_2CH_3)$, PTCS), chloromethyldichloromethylsilane ($Cl_2Si(CH_3)(CH_2Cl)$, CMDCMS), and dimethyldichlorosilane ($Cl_2Si(CH_3)_2$, DMDCS). Calcined MCM-41 (2.0 g) was heated at 180 °C under vacuum (10^{-2} mbar) for 2 h to remove physisorbed water. The dry material was then treated with an excess solution of the organic reagent (2.0 mL) in toluene (30 mL), and the mixture was stirred under reflux for 24 h. The solution was filtered and the residue washed six times with 30 mL aliquots of dichloromethane before drying under vacuum at room temperature for several hours. The silicas functionalized with CMTES, CPTMS, PTCS, CMDCMS, and DMDCS will be referred to as samples **1**, **2**, **3**, **4**, and **5**, respectively. The expected T^n and D^n sites are schematically shown in Figure 1. Not all of these sites were later established (see Figures 2 and 3, and the discussion below).

Solid-State NMR. Experiments were performed at 14.1 and 11.7 T on Varian NMR System 600 (Ames Laboratory) and Bruker DRX-500 (NCL, Pune) spectrometers, equipped with 3.2 and 4 mm MAS probes, respectively. The 2D $^1H-^{29}Si$ and $^1H-^{13}C$ HETCOR experiments were performed using cross polarization and fast MAS for ^1H homonuclear decoupling.[34] The essential experimental parameters are listed below using the following symbols: B_0 denotes the static magnetic field, ν_R the sample rotation rate, ν_{RF}^X the magnitude of radiofrequency magnetic field applied to *X* spins, τ_{CP} the cross polarization time, N_{CPMG} the number of echoes acquired in CPMG experiments, τ_{CPMG} the corresponding time interval between π pulses, τ_{RD} the relaxation delay, and NS the number of scans.

^1H MAS: $B_0 = 14.1$ T; $\nu_R = 0-40$ kHz; $\nu_{RF}^H = 104$ kHz; $\tau_{RD} = 2$ s; NS = 4.

$^1H-^{29}Si$ CPMAS and $^1H-^{29}Si$ HETCOR: $B_0 = 14.1$ T; $\nu_R = 25$ kHz; ν_{RF}^{Si} during CP and CPMG pulses = 55 kHz; ν_{RF}^H during excitation = 104 kHz; ν_{RF}^H during CP = 30 ± 3 kHz (ramped); ν_{RF}^H during TPPM decoupling = 4 kHz; $\tau_{CP} = 8$ ms; $\tau_{CPMG} = 6$ ms; $N_{CPMG} = 160$; $\tau_{RD} = 1$ s.

^{29}Si MAS: $B_0 = 14.1$ T; $\nu_R = 8$ kHz; ν_{RF}^H during TPPM decoupling = 40 kHz; $\tau_{RD} = 300$ s; NS = 300.

$^1H-^{13}C$ HETCOR: $B_0 = 14.1$ T; $\nu_R = 25$ kHz; ν_{RF}^C during CP = 77 kHz; ν_{RF}^H during excitation = 104 kHz; ν_{RF}^H during CP = 52 ± 3 kHz (ramped); ν_{RF}^H during TPPM decoupling = 104 kHz; $\tau_{CP} = 2$ ms; $\tau_{RD} = 1$ s.

^{35}Cl MAS: $B_0 = 11.7$ T; $\nu_R = 5$ kHz; $\nu_{RF}^{Cl} = 20$ kHz; $\tau_{RD} = 0.2$ s; NS = 8000.

The $^1H-^{29}Si$ HETCOR measurements used 100 increments in the t_1 dimension set to 80 μs and CPMG data acquisition. Quadrature detection in the ν_1 dimension was achieved using the hypercomplex method. The number of scans for each of the quadrature components was 80. The total experimental time, which included the acquisition of 160 echoes with $\tau_{CPMG} = 6$ ms, was 9 h per 2D spectrum. The $^1H-^{13}C$ HETCOR experiments used 100 increments (t_1) of 80 μs and 400 scans per increment, which resulted in a total time of hypercomplex acquisition equal to approximately 22 h. In the 2D plots, the consecutive contours reflect 2-fold intensity changes, with the lowest level corresponding to 3% of the maximum intensity in

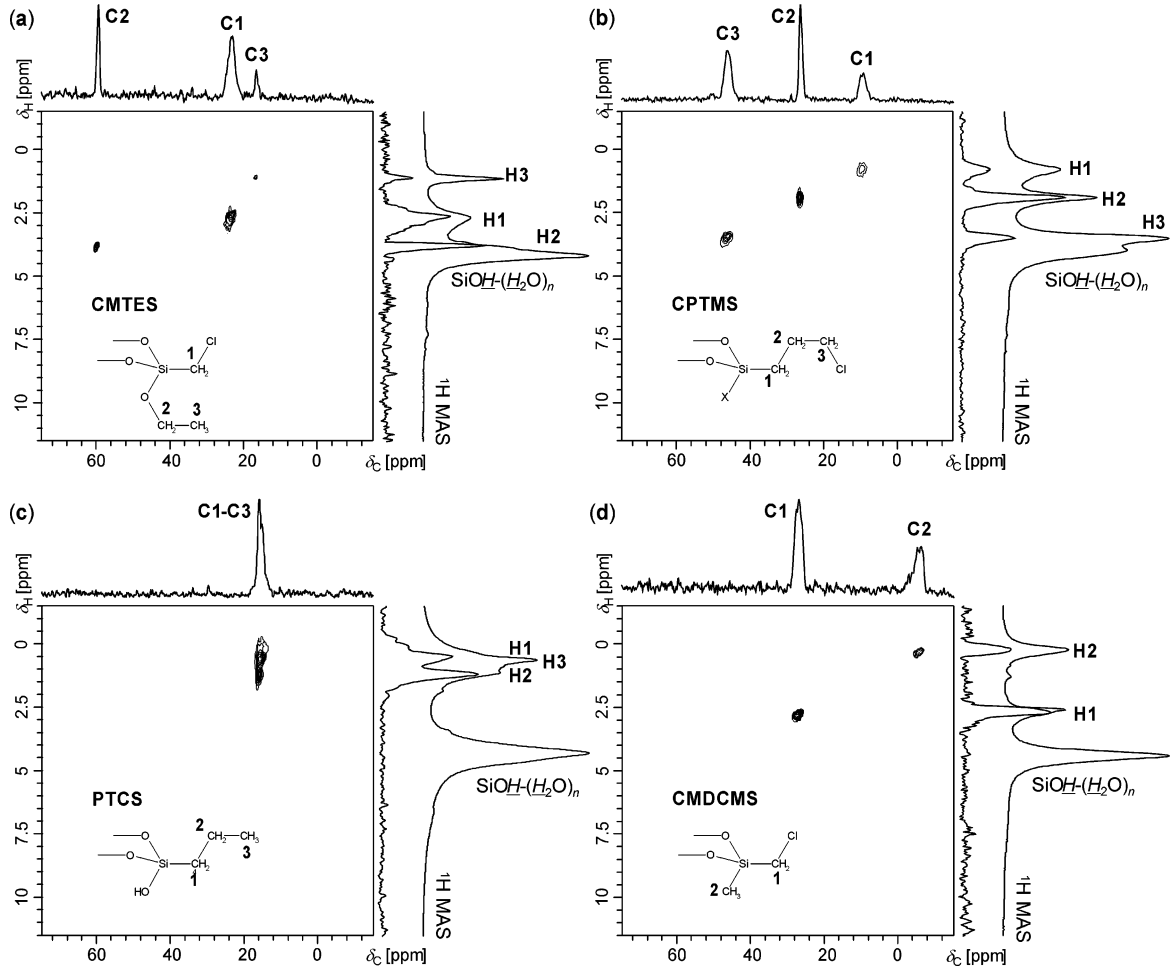

Figure 2. 2D $^{1}H-^{13}C$ HETCOR and the corresponding 1D ^{1}H MAS spectra of samples **1** (a), **2** (b), **3** (c), and **4** (d) acquired under 25 kHz MAS. The spectral assignments are made in reference to the structures shown in the insets. In (b), X denotes OH and/or OCH_3 groups.

most spectra. The 1D projections are shown in skyline mode, normalized to the same heights. The chemical shifts of ^{29}Si, ^{13}C, and ^{1}H are reported using the δ scale and are referenced to tetramethylsilane (TMS) at 0 ppm.

Gaussian 03 Calculations. ^{29}Si, ^{13}C, and ^{1}H chemical shielding tensors were determined using density functional theory as embedded in Gaussian 03.[39] The choice of DFT over the Hartree−Fock method was guided by the increasing versatility and efficiency of the DFT codes due to the availability of more accurate density functionals in Gaussian 03. These enabled calculation of NMR spectral parameters with improved numerical accuracy without undue increase in computational time. The good agreement that DFT yields in ^{29}Si, ^{13}C, and ^{1}H shielding determinations has already been demonstrated in organic and inorganic materials.[40−47] The DFT calculations reported in this paper were carried out using Becke's three-parameter hybrid functional. Molecular clusters representing the various hybrid environments were built using Accelrys Materials Studio molecular modeling software.[48] Charge neutrality of the cluster was ensured by terminating the unconnected Q^2 and Q^3 sites with hydrogens. The structures identified by NMR were geometrically optimized, first using molecular mechanics and then using quantum chemical methods. These optimized local structures were subsequently used for the chemical shielding calculations. Clusters representing Q^2, Q^3, and Q^4 environments of neat MCM-41 were also built and geometrically optimized for comparison with functionalized MCM-41 samples. DFT/B3LYP at the 6-311++G(2d,2p) level was employed for all of the geometry optimizations and the final shielding calculations. The values of ^{29}Si, ^{13}C, and ^{1}H absolute shieldings obtained for σ_{iso} ($^1/_3$ Tr $\boldsymbol{\sigma}$) from Gaussian 03 calculations were converted to relative shifts with respect to TMS and expressed in the δ scale for direct comparison with the experimental data.[49]

Results and Discussion

NMR. The static ^{1}H line widths observed in samples **1**−**5** did not exceed 12 kHz, due to residual molecular motion on the silica surface. As described in the Introduction, fast MAS at 40 kHz proved to be the method of choice in our earlier studies of such moderately coupled spin systems.[33−35] Herein, we used the same experimental heteronuclear correlation schemes as in ref 34, however, at a lower MAS rate of 25 kHz. Although by increasing ν_R to 40 kHz we did observe additional line narrowing by 5−30%,[49] the HETCOR spectra measured at the increased MAS did not reveal any additional structural information in this study. In the $^{1}H-^{13}C$ HETCOR experiments, we applied a π pulse to the ^{13}C spins in the middle of the evolution period in order to refocus the J_{C-H} coupling. Low-power ^{1}H decoupling using TPPM (at $\nu_{RF}^{H} = 4$ kHz) proved to be effective during data acquisition,[34,50,51] which helped to minimize the heating of the probe and the sample during $^{1}H-^{29}Si$ HETCOR experiments with CPMG refocusing.

^{13}C NMR. We show in Figure 2 the 2D $^{1}H-^{13}C$ HETCOR spectra of samples **1**−**4** along with the corresponding skyline projections, as well as the results of 1D ^{1}H MAS measurements. The 1D ^{13}C CPMAS spectra were very similar to the ^{13}C projections of $^{1}H-^{13}C$ HETCOR data and thus are not shown.

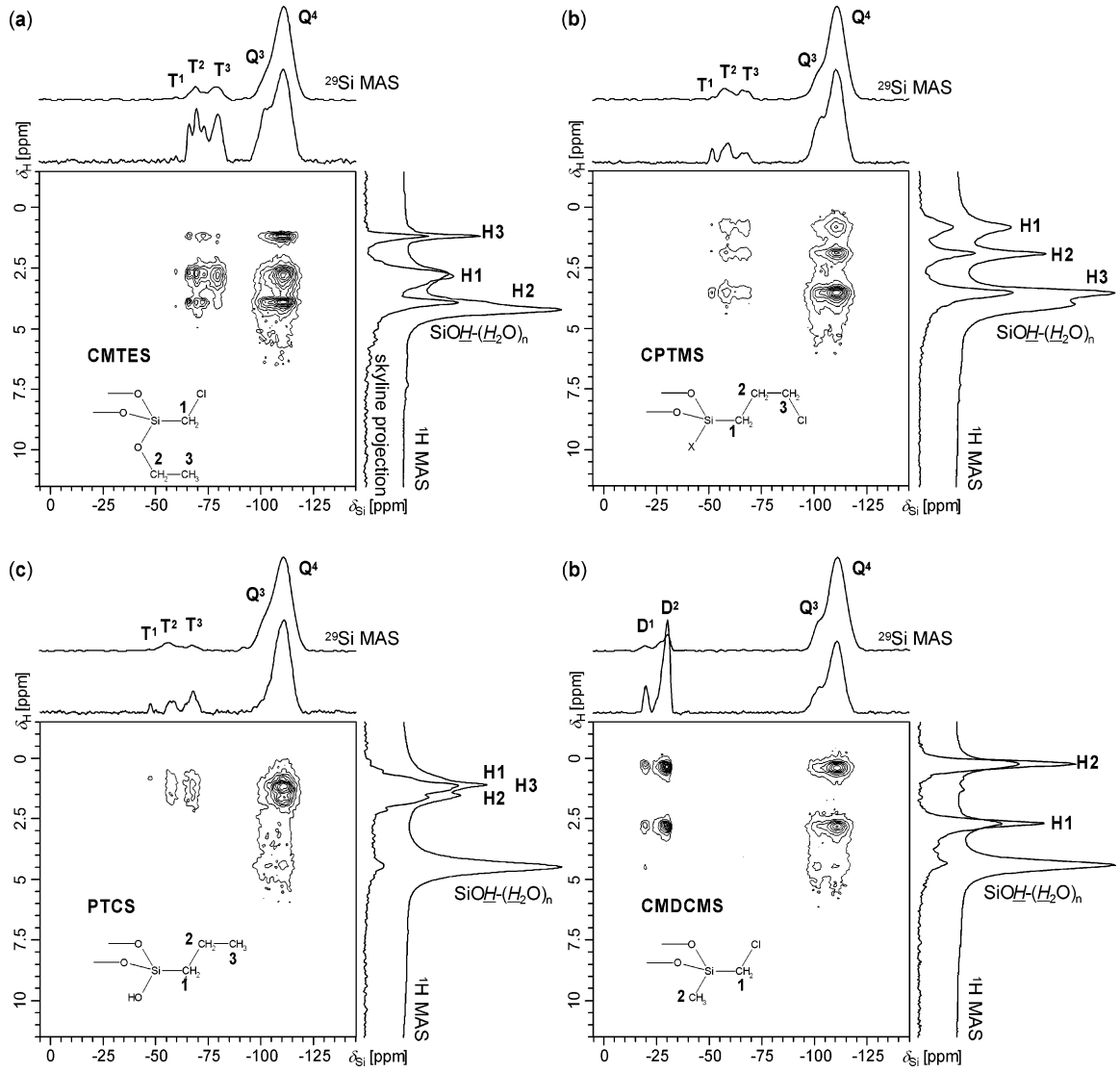

Figure 3. 2D ^{1}H−^{29}Si HETCOR spectra of samples **1** (a), **2** (b), **3** (c), and **4** (d) acquired using CPMG refocusing under 25 kHz MAS. Their skyline projections are compared with the corresponding 1D ^{29}Si and ^{1}H MAS spectra. The spectral assignments are shown in reference to the structures shown in the insets. Again, in (b), X denotes OH and/or OCH_3 groups.

The cross polarization efficiency, although somewhat reduced with respect to fully rigid spin systems due to (restricted) molecular mobility, was consistent with the organic moieties being anchored to the MCM-41 surface. When taken with $\tau_{CP} = 2$ ms, the ^{1}H−^{13}C HETCOR spectra include only correlations between directly bound C−H pairs. The ^{1}H−^{13}C HETCOR spectra feature well resolved resonances which we were able to assign as shown in Figure 2. The results indicate that the MCM-41 silicas were covalently functionalized with CMTES, CPTMS, PTCS, and CMDCMS, as intended. Similarly, the ^{1}H−^{13}C HETCOR spectrum of sample **5**[49] exhibits a single cross-peak at −3 ppm (^{13}C) and 0.3 ppm (^{1}H), as expected for DMDCS. The observed ^{13}C line widths are between 1 and 3 ppm, due to heterogeneity of the functionalized material. Protons that are not associated with carbon are represented by the intense peak at around 3.8−4.5 ppm in the ^{1}H MAS spectra. In our earlier study, this resonance was attributed to water in fast exchange with the residual surface OH groups ($SiOH-(H_2O)_n$ species).[33] Indeed, this intensity vanished upon drying the samples at 100 °C (spectra not shown). The 2D ^{1}H−^{1}H DQ experiments performed under MAS at 25 kHz[49] are fully consistent with the above assignments. Only the ^{1}H−^{1}H DQ correlations within the organic moieties were observed and none with hydrogen on the silica surface.

TABLE 1: Experimental and Calculated ^{13}C Isotropic Chemical Shifts for the T^n and D^n Sites Identified in Organo-Functionalized MCM-41 Silicas 1−5

		T^1/D^1		T^2/D^2		T^3		neat	
	site[a]	exptl	calcd	exptl	calcd	exptl	calcd	exptl	calcd
1	C1	23.5	32.7	23.5	33.7	23.5	34.1	22.2	41.9
	C2	61.4	58.5	61.4	58.9			58.3	62.1
	C3	16.8	14.7	16.8	14.1			17.3	14.8
2	C1	9.6	7.2	9.6	11.1	9.6	11.6	6.5	7.6
	C2	26.7	26.4	26.7	26.8	26.7	26.4	26.3	27.1
	C3	46.3	52.5	46.3	63.9	46.3	63.6	46.8	63.8
	OCH_3	49.2	47.7	49.2	51.1			49.7	51.4
3	C1	14.8	13.2	14.8	13.8	14.8	14.7	26.5	29.4
	C2	14.8	16.7	14.8	15.7	14.8	16.6	16.3	15.9
	C3	14.8	12.0	14.8	12.0	14.8	15.0	15.9	13.8
4	C1	27.6	38.3	27.6	36.8			29.9	38.2
	C2	−6.1	−9.1	−6.1	−7.0			1.96	−0.2
5	C1	−3.9	−5.1	−3.9	−5.1			6.5	−5.1

[a] The carbon sites are denoted as in Figure 2.

In Table 1, the ^{13}C chemical shifts observed in samples **1**−**5** are compared with the signal positions of neat reagents (and

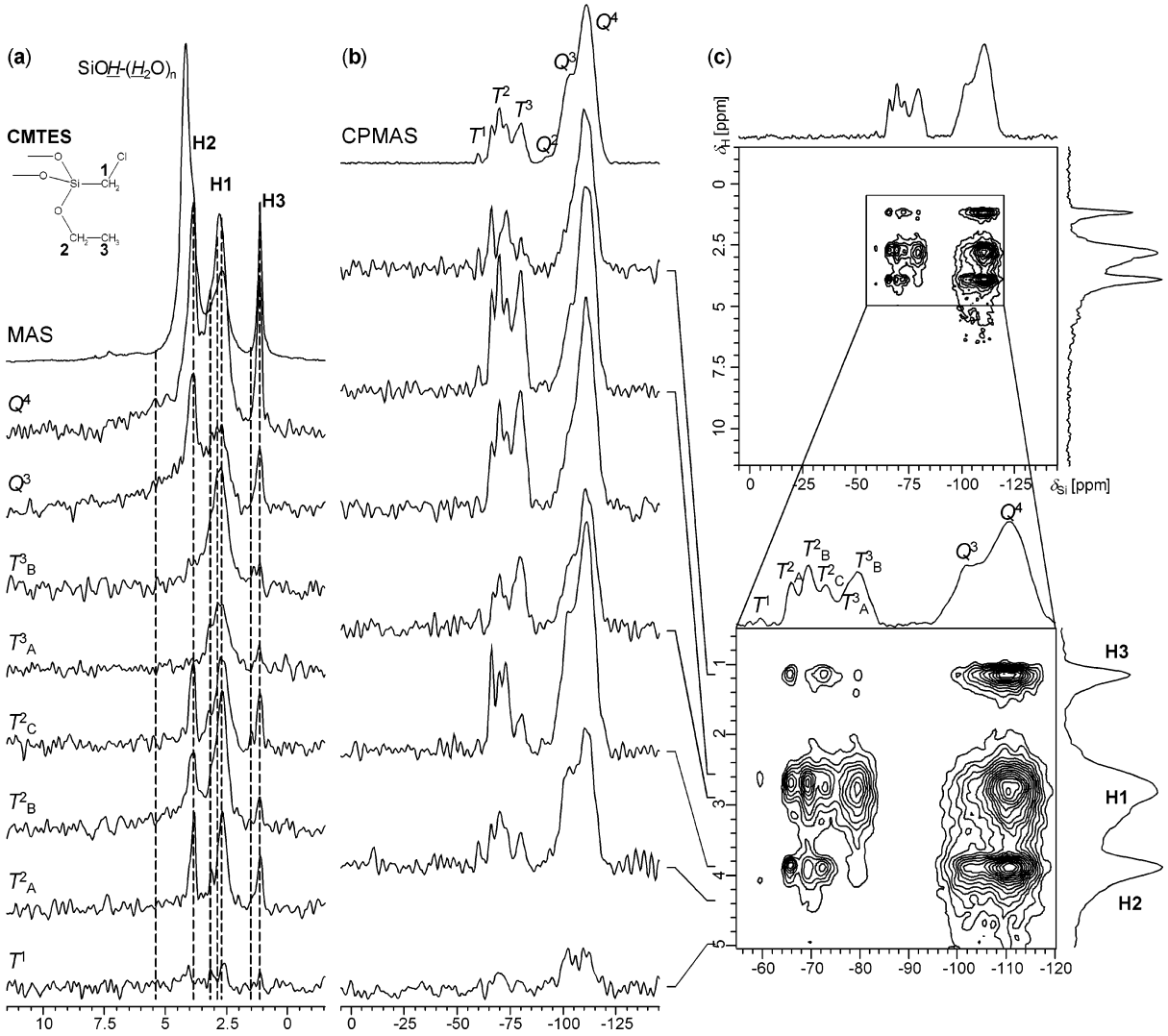

Figure 4. ^{1}H (a) and ^{29}Si (b) cross sections of the ^{1}H−^{29}Si HETCOR spectrum of sample **1** (c).

the calculated values to be discussed later). Clearly, anchoring of the organic ligands to the inorganic host may have a considerable perturbing effect on ^{13}C electronic shielding. As expected, the strongest influence, up to 12 ppm difference in the isotropic chemical shift, was observed for carbons directly attached to the surface in samples **3**−**5**. Further insight into the geometry of these functional groups was provided by the ^{29}Si NMR data discussed below.

^{29}Si NMR. The ^{1}H−^{29}Si HETCOR NMR spectra are shown in Figure 3 (samples **1**−**4**) and in the Supporting Information (sample **5**).[49] As in the case of the ^{1}H−^{13}C measurements, the intensities are derived via a CP process, and thus are inherently dependent on internuclear distances and molecular motion. Additional spectral distortions in the ^{1}H−^{29}Si HETCOR spectra are often introduced during the CPMG data acquisition, due to higher signal enhancement for peaks representing nuclei with longer spin−spin relaxation time (T_2).[34] Under the experimental conditions applied here (160 echoes acquired with ^{1}H decoupling by TPPM), the sensitivity gains were indeed site-dependent, as detailed in the Supporting Information.[49] These factors did not by any means compromise the usefulness of the resulting ^{1}H−^{29}Si HETCOR spectra for structural characterization and were outweighed by the remarkable sensitivity gain which allowed for detailed analysis of the linkages formed on the surface. Also shown in Figure 3 are the results of ^{1}H MAS and ^{29}Si MAS measurements, which are quantitative.

Each of the ^{29}Si spectra is dominated by resonances at around −100 and −110 ppm, representing Q^3- and Q^4-type silicon sites.[24,27,52] Additional peaks are observed with positions, line shapes, and intensities characteristic of the T^n and D^n sites shown in Figure 1. On the basis of the deconvolution of ^{29}Si MAS spectra, we estimated that 15 ± 2, 12 ± 2, 8 ± 2, 9 ± 2, and 9 ± 2% of all silicon atoms in samples **1**−**5**, respectively, are bound to carbon (functionalized). The corresponding concentrations of Q^3 sites, that is, silanol groups that did not react with chloroalkylsilanes, are 14 ± 2, 14 ± 2, 23 ± 3, 10 ± 2, and 12 ± 2%. The relative intensities of all ^{29}Si sites in these samples are given in the Supporting Information.[49] In Table 2, the measured values of ^{29}Si chemical shift are listed along with those observed in nonfunctionalized MCM-41 and in neat alkylsilanes used in this study (the spectra of which are not shown). The resonances representing neat, unattached alkylsilanes were not detected in samples **1**−**5** in measurable concentrations.

The detailed peak assignments can be made by examining the cross sections of ^{1}H−^{29}Si HETCOR spectra in ^{1}H and ^{29}Si dimensions, such as those shown in Figure 4 for sample **1**. The Q^3 and Q^4 sites in all samples are correlated with ^{1}H resonances representing the attached functionalities, which is consistent with the high degree of surface coverage. The fact that these

TABLE 2: Experimental and Calculated ^{29}Si Isotropic Chemical Shifts for the Q^n, T^n, and D^n Sites in MCM-41 and Organo-Functionalized MCM-41 Silicas 1−5

		$n=1$		$n=2$		$n=3$		$n=4$		neat	
	site	exptl	calcd	exptl	calcd	exptl	calcd	exptl	calcd	exptl	calcd
MCM−41	Q^n			−91.8	−104.3	−100.9	−115.2	−110.7	−122.1		
1	T^n			−60.2	−62.8	−69.7	−68.5	−79.6	−71.6	−58.7	−58.8
2	T^n	−50.2	−44.7	−59.0	−60.7	−68.2	−70.8			−43.5	−39.7
3	T^n	−48.1	−33.5	−57.8	−42.8	−67.6	−62.7			12.5	45.8
4	D^n	−20.7	−9.8	−30.0	−19.5					21.0	47.1
5	D^n	−9.2	7.5	−18.5	−3.5					31.8	59.2

correlations include the end groups in CPTMS and PTCS demonstrates that these groups are in close proximity to the surface (no more than 3−4 Å) and are not highly mobile. The Q^3 groups in sample **1** were found to be predominantly of the type $(\equiv SiO)_3$**Si**(OH). Indeed, the hydrogen species $-OH(H_2O)_n$ is (weakly) correlated with Q^3 and Q^4 silicon sites in this sample. The structure of sites represented by resonances in the "T" range is revealed by the ^{1}H cross sections shown in Figure 4a. ^{1}H traces at −80 and −77 ppm, labeled T^3_A and T^3_B, represent hydrogen in CH_2Cl groups, which shows that ^{29}Si resonances T^3_A and T^3_B correspond to $(\equiv SiO)_3$**Si**(CH_2Cl). These two traces are different from those at −73, −69, and −66 ppm, which represent three sites, denoted T^2_A, T^2_B, and T^2_C, that appear to be correlated to both CH_2Cl and ethoxy groups, $(\equiv SiO)_2$**Si**$(CH_2Cl)(OCH_2CH_3)$. There is no clear evidence of correlations between T sites and the hydroxyl groups in this sample, which suggests that the structural differences responsible for the multiplicity of T^2 and T^3 sites can be associated with the presence of different Q and T silicon atoms in the second coordination sphere. Since these small differences will not be explored by DFT calculations, only the average values of chemical shifts corresponding to T^2 and T^3 sites are given in Table 2. (Note that T^2_A and T^2_C sites are less prominent in the ^{29}Si MAS spectrum of Figure 3a. This is due to the aforementioned "T_2 effect", as also demonstrated in Supporting Information, Figure S4c[49]). T^1 sites, which are present in very small concentration, exhibit connectivities consistent with $(\equiv SiO)$**Si**$(CH_2Cl)(OCH_2CH_3)_2$.

The ^{29}Si resonances in other samples can be analyzed and assigned in a similar manner. In the case of CPTMS (sample **2**), T^3 sites are of the $(\equiv SiO)_3$**Si**$(CH_2CH_2CH_2Cl)$ type. The T^2 and T^1 resonances appear to be correlated with the OH groups. However, these sites can also be associated with the methoxy groups, as evidenced by a (weak) resonance at around 49 ppm found in ^{13}C CPMAS spectrum of this sample (not shown). We have earlier detected such groups in the ^{1}H−^{13}C spectrum of functionalized MCM-41 silica at 3.4 and 48 ppm, respectively.[34] Therefore T^2 and T^1 represent $(\equiv SiO)_2$**Si**$(CH_2CH_2CH_2Cl)X$ and $(\equiv SiO)$**Si**$(CH_2CH_2CH_2Cl)X_2$ functionalities, respectively, where X is OH or OCH_3. Sample **3**, as expected, features resonances attributable to the T^3 site $(\equiv SiO)_3$**Si**$(CH_2CH_2CH_3)$ and the T^2 site $(\equiv SiO)_2$**Si**$(CH_2CH_2CH_3)(OH)$ (Figure 3c).

The structures of samples **4** and **5**, functionalized with $Cl_2Si(CH_3)(CH_2Cl)$ (CMDCMS) and $Cl_2Si(CH_3)_2$ (DMDCS), involve D-type sites, with the second organic group being CH_3. Specifically, the more intense peaks at −30 and −19 ppm in samples **4** and **5** are attributed to D^2 groups $(\equiv SiO)_2$**Si**$(CH_3)(CH_2Cl)$ and $(\equiv SiO)_2$**Si**$(CH_3)_2$, whereas the less intense resonances at −21 and −9 ppm represent D^1 groups $(\equiv SiO)$**Si**$(CH_3)(CH_2Cl)(OH)$ and $(\equiv SiO)$**Si**$(CH_3)_2(OH)$, respectively.

It appears from NMR that surface sites having Si−OH rather than Si−Cl linkages were formed in samples **3**−**5**. First, a resonance between silanol proton and D^2 can be discerned in Figure 3d. Second, the presence of Si−Cl bonds should have caused a larger downfield shift, by about 20 ppm,[25] than has been observed in our spectra. Third, these findings are supported by the DFT predicted chemical shifts, as discussed later. Finally, the ^{35}Cl MAS NMR measurements performed at 11.7 T did not reveal any Si−Cl functionalities in these samples.[49] This is an expected result, as the Si−Cl bonds are known to be highly susceptible to hydrolysis.

DFT Calculations of ^{29}Si, ^{13}C, and ^{1}H Chemical Shielding. As described earlier (see Materials and Methods), we have carried out the DFT calculations of ^{29}Si, ^{13}C, and ^{1}H chemical shieldings using cluster models which preserve the local symmetries and coordination geometries around the anchored organic moieties that are consistent with the results obtained by HETCOR NMR. For the five samples studied, the experimental results show that ^{29}Si measurements provide better insights into the nature of linkages between the silica surface and organic moieties than the corresponding ^{13}C measurements. This is mainly attributable to the fact that the covalent linkages

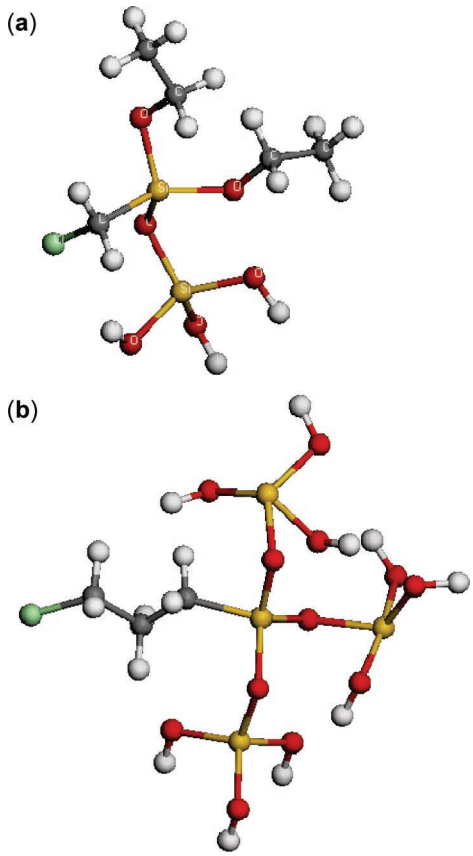

Figure 5. Representative cluster models used for the ab initio calculations of the ^{29}Si, ^{13}C, and ^{1}H chemical shielding tensors. The molecular graphics pictures depict the geometry optimized structures of clusters for samples **1** (a) and **2** (b), functionalized at the T^1 and T^3 sites, respectively.

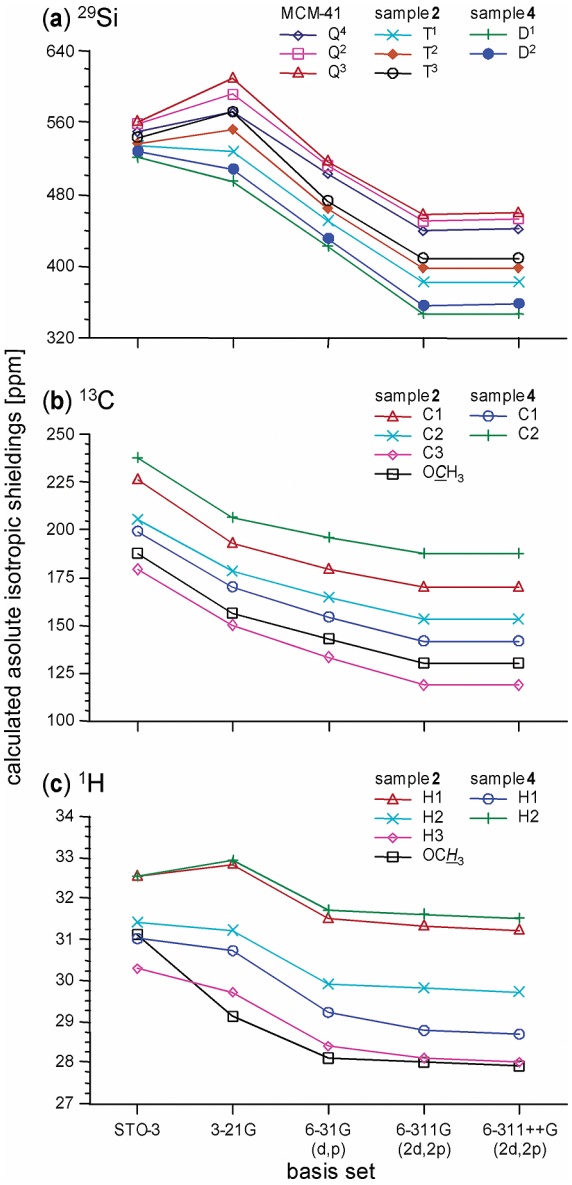

Figure 6. Results of ab initio calculations (DFT/B3LYP) showing the convergence of the isotropic chemical shifts with higher basis sets. The ^{29}Si tests (a) were performed for Q^n sites in nonfunctionalized MCM41 silica, T^n sites in sample **2** (functionalized with CPTMS), and D^n sites in sample **4** (functionalized with CMDCMS). The results of ^{13}C and ^{1}H chemical shift calculations are illustrated for the same samples in parts b and c, where the sites are labeled following the assignments from Figure 2.

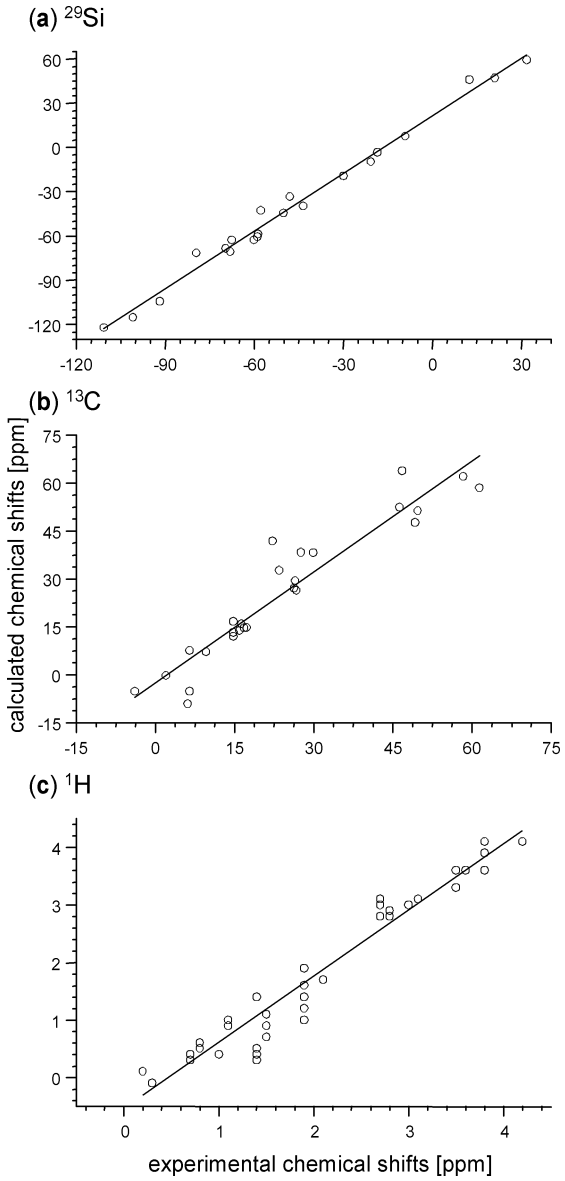

Figure 7. Comparison of the theoretical (DFT/B3LYP/6-311++G(2d,2p)) and experimental isotropic chemical shifts for ^{29}Si (a), ^{13}C (b), and ^{1}H (c) nuclei. The figure includes all data listed in Tables 1−3. The straight lines represent linear least-squares fits to the data.

between carbon and organosilicon remain intact, while the ^{29}Si environments near the surface change considerably. In the case of ^{13}C and ^{1}H, the calculations merely corroborate the assignments which have been made from ^{1}H−^{13}C HETCOR NMR.

The linkages considered for the shielding calculations are those already drafted in Figure 1, with X = OCH_2CH_3 for sample **1**, X = OCH_3 for sample **2**, and X = OH for samples **3**, **4** and **5**. Figure 5 shows a molecular graphics picture of representative geometry optimized clusters. A complete set of illustrations can be found in the Supporting Information.[49] In order to ensure that the B3LYP calculations lead to chemical shielding tensor values of highest possible accuracy, we employed a heavy basis set with the inclusion of diffuse and polarization functions [6-311++G(2d,2p)]. Figure 6 shows typical convergence patterns established in samples **2**, **4**, and nonfunctionalized MCM-41 as the sampling was increased from a sparse STO-3G to a heavy 6-311++G(2d,2p) basis set.

We first discuss the values of ^{29}Si isotropic chemical shifts. The results of ^{29}Si chemical shielding calculations are compiled in Table 2. Also included are the data corresponding to the neat MCM-41 and the organic compounds used. The final DFT results for ^{29}Si sites in samples **1**−**5** are compared with the experimentally determined shifts in Figure 7a. The calculations show excellent correlation with experimental data over the entire range of chemical shifts observed in the neat and functionalized samples, with a reliability coefficient of $R = 0.99$. As expected, they confirm that the isotropic shifts associated with Q^2, Q^3, and Q^4 sites indeed correspond to the chemical shielding increasing in that order. In the case of functionalized environments, the calculations not only predict the chemical shifts in the same order as deduced from NMR but also confirm that there is a partial overlap of the spectral range spanned by some of the signals. On the basis of the DFT calculations of the ^{29}Si chemical shielding, the functionalized environments T^1, T^2, and

TABLE 3: Experimental and Calculated ^{1}H Isotropic Chemical Shifts for the T^n and D^n Sites Identified in Organo-Functionalized MCM-41 Silicas 1−5

		T^1/D^1		T^2/D^2		T^3		neat	
	site[a]	exptl	calcd	exptl	calcd	exptl	calcd	exptl	calcd
1	H1	2.7	3.0	2.7	2.8	2.7	3.1	3.1	3.1
	H2	3.8	4.1	3.8	3.9			4.2	4.1
	H3	1.1	1.0	1.1	0.9			1.5	1.1
2	H1	0.7	0.3	0.7	0.4	0.7	0.4	1.0	0.4
	H2	1.9	1.6	1.9	1.9	1.9	1.9	2.1	1.7
	H3	3.5	3.3	3.5	3.6	3.5	3.6	3.8	3.6
	OCH_3	3.6	3.6	3.6	3.6			3.5	3.6
3	H1	1.4	0.5	1.4	0.4	1.4	0.3	1.1	1.0
	H2	1.9	1.4	1.9	1.2	1.9	1.0	1.4	1.4
	H3	1.5	0.9	1.5	0.7	1.5	0.7	0.8	0.6
4	H1	2.8	2.9	2.8	2.8			3.0	3.0
	H2	0.2	0.1	0.2	0.1			0.8	0.5
5	H3	0.3	−0.1	0.3	−0.1			0.7	0.4

[a] The proton sites are denoted as in Figures 2 and 3.

T^3 in samples **1**, **2**, and **3**, which represent sites with covalent linkages to the organic moieties through one, two, and three bridging oxygens, respectively, are duly represented in the scheme of Figure 1 (with X being OH, OCH_3, or OCH_2CH_3). For samples **4** and **5**, the ^{29}Si resonances representing functionalized sites are deshielded with respect to samples **1**, **2**, and **3**. The D^1 and D^2 sites in sample **5** occur at the deshielding extreme, which is well reflected by the calculations.

The final results of the ^{13}C and ^{1}H ab initio calculations and their comparison with the ^{13}C CPMAS and ^{1}H MAS results for the three functionalized MCM-41 samples are listed in Tables 1 and 3 and illustrated in parts b and c of Figure 7, respectively. The ^{13}C calculations reproduce the observed trend in chemical shifts for both neat compounds and functionalized hybrid materials with an R value of 0.95. A better yet correlation is observed in the case of ^{1}H shifts ($R = 0.96$). Since the carbon atoms are more displaced from the MCM lattice than organosilicon, small differences in ^{1}H and ^{13}C shifts induced by functionalization to different types of T sites or D sites cannot be experimentally detected under the resolution that these samples afford. Similarly, such fine differences in ^{13}C chemical shifts cannot be reproduced in our calculations because of the ∼5 ppm uncertainty at the B3LYP (6-311++G(2d,2p)) level. Nevertheless, the large chemical shift dispersion caused by the different chemical environments is well reproduced both in the experiments and in the calculations.

Conclusion

We have demonstrated that state-of-the-art solid-state NMR experiments and calculations can be used in concert to characterize the complex structures of mesoporous inorganic−organic hybrid materials. We found that there is an excellent correspondence between the experimental and theoretically calculated isotropic chemical shifts for ^{29}Si, ^{13}C, and ^{1}H nuclei. The small deviations of the least-squares fit lines from the slope of unity and from intercepting zero indicate overall systematic errors, which are typically encountered in such calculations.[53] These mainly arise in DFT methods due to under- or overestimation of the electronic correlation effects on the calculated shielding constants for the chosen molecular systems and the reference compound (TMS). The usefulness of such methods in the studies of hybrid materials is expected to increase with further development of both experimental and theoretical capabilities.

Acknowledgment. Financial assistance from Reliance Industries Limited, Mumbai, India, is gratefully acknowledged. At Ames Laboratory, this research was supported by the U.S. DOE, office of BES, under contract W-7405-Eng-82. The authors are indebted to Drs. B. C. Gerstein, M. S. Gordon, P. R. Rajamohanan, and T. G. Ajithkumar for helpful discussions and to Gurpreet Singh for computational assistance.

Supporting Information Available: Additional NMR data: ^{1}H spectra of sample **1** as a function of MAS frequency, ^{1}H MAS spectra of all samples acquired at 25 kHz, ^{1}H−^{13}C and ^{1}H−^{29}Si HETCOR spectra of sample **5**, ^{1}H−^{1}H double-quantum spectra of samples **1**−**4**, a plot of signal-to-noise gain versus N_{CPMG} for sample **1**, and ^{35}Cl MAS spectra of all samples. Also included are the cluster models for samples **1**−**5** and a table with ^{29}Si, ^{13}C, and ^{1}H absolute shielding values for TMS utilized for converting isotropic shieldings to chemical shift scale. This material is available free of charge via the Internet at http://pubs.acs.org.

References and Notes

(1) Dai, S.; Burleigh, M. C.; Shin, Y.; Morrow, C. C.; Barnes, C. E.; Xue, Z. *Angew. Chem., Int. Ed. Engl.* **1999**, *38*, 1235−1239.
(2) Yoshitake, H.; Yokoi, T.; Tatsumi, T. *Chem. Mater.* **2003**, *15*, 1713−1721.
(3) Hossain, K. Z.; Mercier, L. *Adv. Mater.* **2002**, *14*, 1053−1056.
(4) Lai, C.-Y.; Trewyn, B. G.; Jeftinija, D. M.; Jeftinija, K.; Xu, S.; Jeftinija, S.; Lin, V. S. Y. *J. Am. Chem. Soc.* **2003**, *125*, 4451−4459.
(5) Lin, V. S. Y.; Lai, C.-Y.; Huang, J.; Song, S.-A.; Xu, S. *J. Am. Chem. Soc.* **2001**, *123*, 11510−11511.
(6) Burleigh, M. C.; Dai, S.; Hagaman, E. W.; Lin, J. S. *Chem. Mater.* **2001**, *13*, 2537−2546.
(7) Soler-Illia Galo, J. d. A. A.; Sanchez, C.; Lebeau, B.; Patarin. J. *Chem. Rev.* **2002**, *102*, 4093−4138.
(8) Davis, M. E. *Nature* **2002**, *417*, 813−821.
(9) Corma, A. *Chem. Rev.* **1997**, *97*, 2373−2419.
(10) Price, P. M.; Clark, J. H.; Macquarrie, D. J. *Dalton* **2000**, 101−110.
(11) Ying, J. Y.; Mehnert, C. P.; Wong, M. S. *Angew. Chem., Int. Ed.* **1999**, *38*, 56−77.
(12) Moller, K.; Bein, T. *Chem. Mater.* **1998**, *10*, 2950−2963.
(13) Huh, S.; Chen, H.-T.; Wiench, J. W.; Pruski, M.; Lin, V. S. Y. *J. Am. Chem. Soc.* **2004**, *126*, 1010−1011.
(14) Huh, S.; Chen, H.-T.; Wiench, J. W.; Pruski, M.; Lin, V. S. Y. *Angew. Chem., Int. Ed.* **2005**, *44*, 1826−1830.
(15) Kresge, C. T.; Leonowicz, M. E.; Roth, W. W.; Vartuli, J. C.; Beck, J. S. *Nature* **1992**, *359*, 710−712.
(16) Liu, J.; Shin, Y.; Nie, Z.; Chang, J. H.; Wang, L. Q.; Fryxell, G. E.; Samuels, W. D.; Exarhos, G. J. *J. Phys. Chem. A* **2000**, *104*, 8328−8339 and references therein.
(17) Lim, M. H.; Stein, A. *Chem. Mater.* **1999**, *11*, 3285−3295.
(18) Stein, A.; Melde, B. J.; Schroden, R. C. *Adv. Mater.* **2000**, *12*, 1403−1419.
(19) Fowler, C. E.; Burkett, S. L.; Mann, S. *Chem. Commun.* **1997**, 1769−1770.
(20) Lim, M. H.; Blanford, C. F.; Stein, A. *J. Am. Chem. Soc.* **1997**, *119*, 4090−4091.
(21) Moller, K.; Bein, T.; Fischer, R. X. *Chem. Mater.* **1999**, *11*, 665−673.
(22) Inagaki, S.; Guan, S.; Ohsuna, T.; Terasaki, O. *Nature* **2002**, *416*, 304−307.
(23) Huh, S.; Wiench, J. W.; Trewyn, B. G.; Song, S.; Pruski, M.; Lin, V. S. Y. *Chem. Commun.* **2003**, 2364−2365.
(24) Huh, S.; Wiench, J. W.; Yoo, J.-C.; Pruski, M.; Lin, V. S. Y. *Chem. Mater.* **2003**, *15*, 4247−4256.
(25) Marsmann, H. C. Silicon-29 NMR. In *Encyclopedia of Nuclear Magnetic Resonance*; Grant, D. M., Harris, R. K., Eds.; John Wiley & Sons Ltd: Chichester, U.K., 1996; Vol. 7, pp 4386−4398.
(26) Janicke, M. T.; Landry, C. C.; Christiansen, S. C.; Kumar, D.; Stucky, G. D.; Chmelka, B. F. *J. Am. Chem. Soc.* **1998**, *120*, 6940−6951.
(27) Maciel, G. E. Silica Surfaces: Characterization. In *Encyclopedia of Nuclear Magnetic Resonance*; Grant, D. M., Harris, R. K., Eds.; John Wiley & Sons Ltd: Chichester, U.K., 1996; Vol. 7, pp 4370−4386.
(28) Brown, S. P.; Spiess, H. W. *Chem. Rev.* **2001**, *101*, 4125−4155.
(29) Chen, C. Y.; Li, H. X.; Davis, M. E. *Microporous Mater.* **1993**, *2*, 17−26.

(30) Asefa, T.; Kruk, M.; Coombs, N.; Grondey, H.; MacLachlan, M. J.; Jaroniec, M.; Ozin, G. A. *J. Am. Chem. Soc*. **2003**, *125*, 11662−11673.
(31) Kwak, J. H.; Herrera, J. E.; Hu, J. Z.; Wang, Y.; Peden, C. H. F. *Appl. Catal., A* **2006**, *300*, 109−119.
(32) Stein, A.; Fendorf, M.; Jarvie, T. P.; Mueller, K. T.; Benesi, A. J.; Mallouk, T. E. *Chem. Mater.* **1995**, *7*, 304−13.
(33) Trebosc, J.; Wiench, J. W.; Huh, S.; Lin, V. S. Y.; Pruski, M. *J. Am. Chem. Soc*. **2005**, *127*, 3057−3068.
(34) Trebosc, J.; Wiench, J. W.; Huh, S.; Lin, V. S. Y.; Pruski, M. *J. Am. Chem. Soc*. **2005**, *127*, 7587−7593.
(35) Chen, H.-T.; Huh, S.; Wiench, J. W.; Pruski, M.; Lin, V. S. Y. *J. Am. Chem. Soc*. **2005**, *127*, 13305−13311.
(36) Nunes, C. D.; Valente, A. A.; Pillinger, M.; Fernandes, A. C.; Romão, C. C.; Rocha, J.; Gonçalves, I. S. *J. Mater. Chem*. **2002**, *12*, 1735−1742.
(37) Maity, N.; Basu, S.; Mapa, M.; Rajamohanan, P. R.; Ganapathy, S.; Gopinath, C. S.; Bhaduri, S.; Lahiri G. K. *J. Catal.* **2006**, *242*, 332−339.
(38) Beck, J. S.; Vartuli, J. C.; Leonowicz, M. E.; Kresge, C. T.; Schmitt, K. D.; Chu, C. T. W.; Olson, D. H.; Sheppard, E. W.; McCullen, S. B.; Higgins, J. B.; Schlenker, J. L. *J. Am. Chem. Soc.* **1992**, *114*, 10834−10843.
(39) Frisch, M. J.; Trucks, G. W.; Schlegel, H. B.; Scuseria, G. E.; Robb, M. A.; Cheeseman, J. R.; Zakrzewski, V. G.; Montgomery, J. A.; Stratmann, R. E.; Burant, J. C.; Dapprich, S.; Millam, J. M.; Daniels, A. D.; Kudin, K. N.; Strain, M. C.; Farkas, O.; Tomasi, J.; Barone, V.; Cossi, M.; Cammi, R.; Mennucci, B.; Pomelli, C.; Adamo, C.; Clifford, S.; Ochterski, J.; Petersson, G. A.; Ayala, P. Y.; Cui, Q.; Morokuma, K.; Rega, N.; Salvador, P.; Dannenberg, J. J.; Malick, D. K.; Rabuck, A. D.; Raghavachari, K.; Foresman, J. B.; Cioslowski, J.; Ortiz, J. V.; Baboul, A. G.; Stefanov, B. B.; Liu, G.; Liashenko, A.; Piskorz, P.; Komaromi, I.; Gomperts, R.; Martin, R. L.; Fox, D. J.; Keith, T.; Al-Laham, M. A.; Peng, C. Y.; Nanayakkara, A.; Challacombe, M.; Gill, P. M. W.; Johnson, B.; Chen, W.; Wong, M. W.; Andres, J. L.; Gonzalez, C.; Head-Gordon, M.; Replogle, E. S.; Pople, J. A. *Gaussian 03*, revision A.11.2; Gaussian, Inc.: Pittsburgh, PA, 2001.
(40) Tsantes, G.; Auner, N.; Muller, T. In *Organosilicon Chemistry V*; Auner, N., Weis, J., Eds.; VCH: Weinheim, Germany, 2003; p 334.
(41) Valerio, G.; Goursot, A.; Vetrivel, R.; Malkina, O.; Malkin, V.; Salahub, D. R. *J. Am. Chem. Soc*. **1998**, *120*, 11426−11431.
(42) Bull, L. M.; Bussemer, B.; Anupold, T.; Reinhold, A.; Samoson, A.; Sauer, J.; Cheetham, A. K.; Dupree, R. *J. Am. Chem. Soc.* **2000**, *122*, 4948−4958.
(43) Xue, X.; Kamzaki, M. *Solid State Nucl. Magn. Reson.* **2000**, *16*, 245−259.
(44) Jameson, C. J.; de Dios, A. C. *A Specialist Periodic Report*; The Royal Society of Chemistry: London, 1999; Vol. 28, pp 42−76.
(45) Alkorta, I.; Elguero, J. *Magn. Reson. Chem.* **2004**, *42*, 955−961.
(46) Kupka, T.; Pastema, G.; Lodowski, P.; Szeja, W. *Magn. Reson. Chem.* **1999**, *37*, 421−426.
(47) Barone, G.; Gomez-Paloma, L.; Duca, D.; Silvestri, A.; Riccio, R.; Bifulco, G. *Chem.—Eur. J.* **2002**, *8*, 3233−3239.
(48) *Materials Studio Modeling Software 3.0*; Accelrys Ltd: Cambridge, U.K.
(49) See the Supporting Information for details.
(50) Bennett, A. E.; Rienstra, C. M.; Auger, M.; Lakshmi, K. V.; Griffin, R. G. *J. Chem. Phys*. **1995**, *103*, 6951−6958.
(51) Ernst, M.; Samoson, A.; Meier, B. H. *Chem. Phys. Lett*. **2001**, *348*, 293−302.
(52) Engelhardt, G.; Michel, D. *High-Resolution Solid-State NMR of Silicates and Zeolites*; John Wiley & Sons: Chichester, U.K., 1987.
(53) Facelli, J. C., Chemical Shielding Calculations. In *Encyclopedia of Nuclear Magnetic Resonance*; Grant, D. M., Harris, R. K., Eds.; John Wiley & Sons Ltd: Chichester, U.K., 2002; Vol. 9 (Advances in NMR), pp 323−333.